6

Simulation of compression moulding to form composites

E SCHMACHTENBERG, Universität Erlangen-Nürnberg, Germany
and K SKRODOLIES, Institut für Kunststoffverarbeitung, Germany

6.1 Introduction

Fibre reinforced compression moulding parts are well established in industry. One can distinguish between two main types of these compounds.

Thermoset compression moulding prepregs (so-called sheet moulding compounds, SMC) were established in the early 1960s. The compression moulding process of these materials starts with the rapid closing of a mould followed by squeezing the prepreg into its final shape. The charge temperature is about room temperature, the mould temperature ranges from 120 to 150ºC (Ehrenstein 1992). The temperature of the compound rises during the flow due to the heat transfer from the cavity surfaces. Due to this, the viscosity declines before the cross linking reaction starts (Neitzel and Breuer 1996). Local gradients of pressure in the mould cause different local velocities and fibre orientations during the flow. These orientations affect the anisotropy of the part. Besides the thermal process parameters, it is the flow that has a major influence on the part properties.

Thermoplastic compression moulding compounds (GMT) were invented twenty years after the establishment of SMC. The main difference concerning the process is that these compounds are heated up to melting temperature in a heating station or extruder and put into a 'cold' mould (mould temp. 60–80ºC). Due to the withdrawal of heat in the mould the material starts to freeze right after deposition and during the flow in the mould. Thus, the material properties are influenced by the thermal process parameters and the local pressure/velocity gradients, analogously to the thermoset materials.

Hence, the manufacturer of compression moulding parts has a great responsibility to find the optimal process parameters. Therefore, a numeric simulation of the compression moulding process is a very important tool to save time and costs. Only by using this tool it is possible to assess alternative concepts in an early construction phase.

In other areas of plastics processing, e.g. injection moulding, the use of process simulation software is very common. Unlike this, such programs are only little used in the field of compression moulding despite the complexity of the processes and materials. In cooperation between the IKV and M-Base Engineering + Software GmbH, Aachen, the process-simulation software EXPRESS has been developed and constantly been improved (Specker 1990, Heber 1995, Semmler 1998). This program contains several modules: First there was the Newtonian flow simulation, which gives information on the flow in the cavity (Specker 1990). Afterwards other modules were integrated like the fibre orientation computation with an interface to FE-programs. With this, one gets the possibility of a FE-analysis regarding the anisotropic rigidity and the possibility of failure analysis. With this knowledge a calculation of shrinking and warpage of the parts could be done.

A disadvantage of the Newtonian flow is that the material properties (e.g., the temperature dependence of the viscosity) are not described. Therefore, a non Newtonian flow model was integrated (Heber 1995) which is based on a Hele-Shaw flow-law as it is successfully used in various injection moulding simulation programs. With the use of a temperature dependent non Newtonian flow model the local pressure ratios in the cavity can be calculated at each time step. This leads to an exact calculation of the local velocities and the velocity gradients, which are an input for the fibre orientation computation. Furthermore, the local pressure is used to calculate the pressing force and the movement of the centre of force.

These results give the manufacturer an exact knowledge of the whole process. Additional to the existing know-how of the manufacturer further conclusions can be drawn depending on the results of the simulation (Schmachtenberg and Ritter 2002). This opens new prediction possibilities for parts with high requirements on surface quality. Additionally, it can be estimated if the existing presses can be used to manufacture the new parts or if a new investment is necessary.

6.2 Theoretical description of the simulation

6.2.1 Flow and heat transfer simulation

The following section gives an overview of the methods used to simulate the fluid and energy flow during processing. At first the calculation of an isothermal flow will be shown, that will be extended to a non-isothermal flow calculation. This mode can be used for the flow simulation for both thermoplastic and thermoset materials if the freezing of material is taken into account.

With the isothermal flow calculation you have a quantitatively less accurate prediction of the flow behaviour compared to the non-isothermal simulation. However, with the advantage being that computational time is significantly decreased. In the case that the properties of the simulated material are highly

temperature dependent and you are concerned with obtaining a more accurate prediction of shrinkage, warpage and the final material properties for the part, a non-isothermal flow calculation is recommended.

Isothermal flow simulation

The simplified forms of the conservation of mass (eq. 6.1) and momentum (eq. 6.2) given below describe the flow of isothermal, Newtonian, incompressible fluids, and serve as the rheological foundations of the flow simulation (Renz 1989).

$$\nabla \bar{v} = 0 \tag{6.1}$$

$$\rho\left(\frac{\partial \bar{v}}{\partial t} + (\bar{v}\nabla)\bar{v}\right) = \rho\bar{g} - \nabla\bar{\sigma} - \nabla p \tag{6.2}$$

The governing equations above can be further simplified for the compression moulding process based on the application of the Hele-Shaw model (Hele-Shaw and Stirling 1899), for which the following assumptions must be fulfilled (Osswald 1987):

1. The inertial forces are insignificant with respect to the viscous forces and can be neglected.
2. The flow is isotropic, incompressible, and the velocities at the mould walls are always equal to zero (no-slip assumption).
3. The effects of gravity and surface tension can be neglected.
4. The elastic forces are insignificant with respect to the viscous forces and can be neglected.
5. Drag flow is insignificant with respect to pressure induced flow and can be neglected.
6. The fluid can be assumed to have Newtonian behaviour and is dominated by shear flow.
7. The assumptions required to apply laminate theory are valid for the considered geometries (the part thickness is significantly smaller than the other part dimensions).

Applying the assumptions above to eqs. 6.1 and 6.2 and arranging the variables in a specific form leads to the following differential equation describing the time-dependent pressure distribution during processing (Osswald 1987, Heber 1995):

$$\frac{\partial}{\partial x}\left(S\frac{\partial p}{\partial x}\right) + \frac{\partial}{\partial y}\left(S\frac{\partial p}{\partial y}\right) - \dot{h} = 0 \tag{6.3}$$

The variable S in eq. 6.3 is defined as the flow conductivity and is a function of the material viscosity as well as the transient flow channel height. For

isothermal, Newtonian fluids the flow conductivity reduces to the following expression:

$$S = \frac{h^3}{12\eta} \qquad 6.4$$

Equation 6.3 can be solved numerically for the pressure distribution at each time step from which the instantaneous velocities can be derived. The following boundary conditions are required to obtain a solution to eq. 6.3:

1. The pressure at the flow front is equal to zero in all unfilled regions.
2. The pressure gradient perpendicular to the top and bottom halves of the mould wall is zero (the material is not allowed to squeeze out of the mould cavity where the two mould halves come together).

Equation 6.3 can be solved by using the finite element method. A widespread approach to describe the flow of the material in the calculation is the control volume approach (Osswald 1987). This approach accounts for the movement of the flow front by defining a control volume mesh that is based on a static mesh. The flow front progression is followed into and out of the control volumes by defining a filling factor. Figure 6.1 shows a simplified representation of the relationship between the finite element mesh and the control volume mesh along with the behaviour of the filling factor as the flow front progresses through the control volumes.

Contrary to the assumptions above, process conditions in the compression moulding process are not isothermal. In the case of thermoset materials, the temperature of the charge is about 25ºC and the mould temperature about 120ºC to 150ºC. Thermoplastic materials were put with melt temperature (approx.

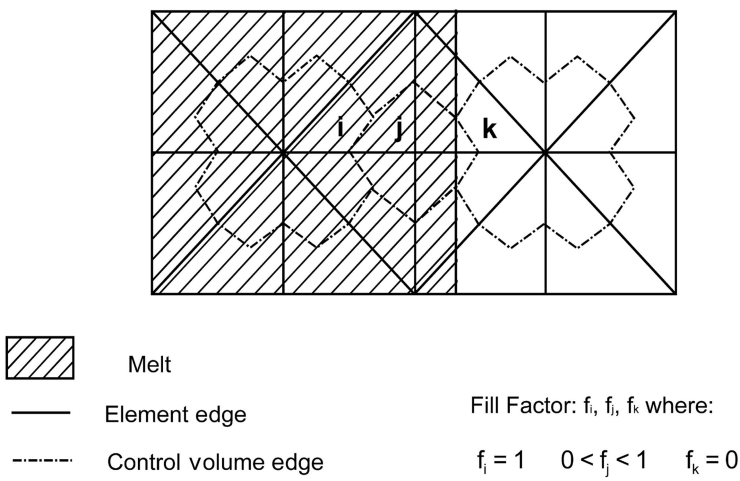

6.1 Control volume principle.

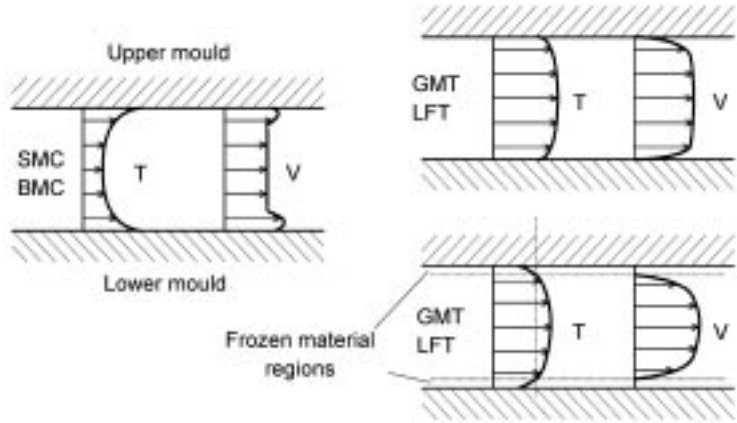

6.2 Compression moulding flow phenomena for SMC-BMC and GMT-LFT.

200ºC to 250ºC at materials with a PP matrix) in a cold mould (temperature 60ºC to 80ºC). Due to the strong dependency of the viscosity on the material temperature there is a big difference between the results of an isothermal simulation and the non-isothermal process. The temperature and velocity distribution for these two polymer families are shown in Fig. 6.2. Therefore a non-isothermal flow simulation considering the temperature change of the material during the flow and the dependency of the viscosity on the material temperature and the shearing rate as well is more accurate. Only with the non-isothermal simulation predictions of the local pressures are the pressing force and the local fibre orientation distribution helpful.

Non-isothermal flow simulation

As mentioned previously, a non-isothermal flow simulation models the actual process more accurately compared to an isothermal flow simulation. One model to describe the influence of the temperature and shear rate on the viscosity of the material is the Carreau-WLF model (eq. 6.5 and 6.6) (Heber 1995, Carreau 1968, Williams *et al.* 1955).

$$\eta = \frac{P_1 a_T}{(1 + a_T P_2 |\dot{\gamma}|)^{P_3}} \qquad 6.5$$

$$\log(a_T) = \frac{8.86(T_B - T_S)}{101.6°\mathrm{C} + (T_B - T_S)} - \frac{8.86(T - T_S)}{101.6°\mathrm{C} + (T - T_S)} \qquad 6.6$$

The shear rate, $\dot{\gamma}$, corresponds to the velocity gradient through the flow channel height, while the temperature shift coefficient, a_T, accounts for the variation of the viscosity at various temperatures. At this point it becomes apparent that modelling the heat flow during the compression moulding process is necessary.

The simulation of the energy transport is also used in the latter stages of the program to calculate the temperature dependent material properties as well as the development of internal stresses.

6.2.2 Heat transfer simulation

Energy transport during the filling stage

Because the filling stages of the compression moulding process are strongly temperature dependent, the calculation of the temperature distribution is an essential step in the simulation of the process. Eq. 6.7 gives the simplified form of the energy equation used in the simulation of the heat transfer:

$$\begin{aligned} \rho c_p \frac{\partial T}{\partial t} &= \gamma \frac{\partial^2 T}{\partial z^2} && \text{Conduction} \\ -\rho c_p \left(v_x \frac{\partial T}{\partial x} + v_y \frac{\partial T}{\partial y} \right) & && \text{Convection} \\ -\tau_{xz} \frac{\partial v_x}{\partial z} - \tau_{yz} \frac{\partial v_y}{\partial z} & && \text{Diffusion} \end{aligned} \qquad 6.7$$

The equation above was derived using the following assumptions:

1. Conduction heat transfer only occurs in the through-thickness direction.
2. Convection heat transfer only occurs in the direction of material flow.
3. The temperature profile is symmetric.
4. The heat transfer between the material and the mould walls is ideal, resulting in a constant mould temperature throughout the filling stage.
5. In the case where a thermoset is being simulated, it is assumed that the material begins to cure only after the entire mould has been filled.

The validity of the assumptions used in the application of the Hele-Shaw model as well as the simplification of the energy equation are validated in (Heber 1995). The simplified energy equation is then solved in conjunction with the governing flow equation, where the non-linear viscosity acts to connect the two governing equations to one another. This, however, increases the complexity of the simulation, meaning that the calculation time significantly increases.

Energy transport during and after the filling stage

After the mould has been completely filled the convection and diffusion terms in the above energy equation drop out, leaving the single conduction term on the right-hand side of the equation. If a thermoset is being simulated, then the source term (responsible for accounting for the heat generation during curing) must be reintroduced. However, overall the energy equation becomes simpler, meaning that a less rigorous method can be applied to solve this equation, saving the unnecessary expenditure of computational time.

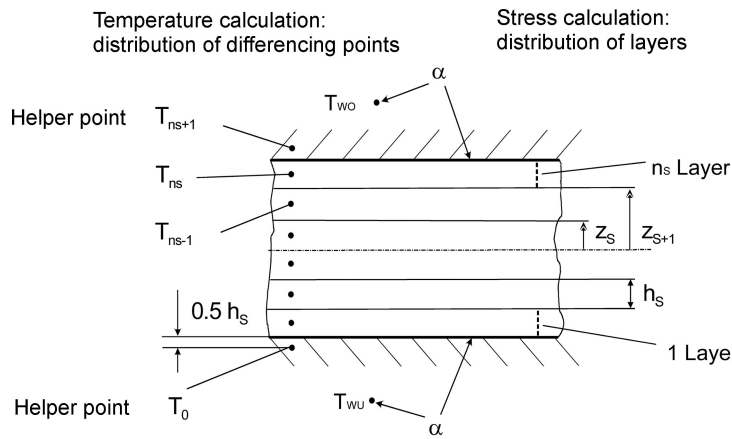

6.3 Through-thickness discretisation.

Based on this argument, the energy transport in the second part of the simulation is solved using one-dimensional implicit finite difference method. In order to use this method, additional finite difference points need to be defined in the through-thickness direction of the part. These points are located in the middle of each of the ten defined stress layers (this will be discussed later in the section on thermomechanical theory), along with two extra points, called the 'helper points', located outside of the geometry. These 'helper points' will be used in the shrinkage and warpage module to calculate the additional warpage due to the influence of corners within a part. Figure 6.3 schematically shows the placement of these points through the thickness of the part geometry.

The solution of the differential equation requires that it is first converted into a finite difference form using the following substitutions:

$$\frac{\partial T_S}{\partial t} = \frac{T_{S,k+1} - T_{S,k}}{\Delta t} \tag{6.8}$$

and:

$$\frac{\partial^2 T_S}{\partial z^2} = \frac{\dfrac{T_{S+1,k+1} - T_{S,k+1}}{h_S} - \dfrac{T_{S,k+1} - T_{S-1,k+1}}{h_S}}{h_S} \tag{6.9}$$

$$\frac{\partial^2 T_S}{\partial z^2} = \frac{T_{S+1,k+1} - 2T_{S,k+1} + T_{S-1,k+1}}{h_S^2} \tag{6.10}$$

In the case of thermosets the development of heat due to curing must also be included in the solution of the energy transport. The degree of cure $c_{S,k}$ for a stress layer S at a time k is defined as the current heat energy released divided by the total heat energy available. The rate of heat generation can then derived by differentiating the rate of cure with respect to time, or symbolically as:

$$c_{S,k} = \frac{Q_{S,k}}{Q_g} \rightarrow Q_{S,k} = Q_g c_{S,k} \rightarrow \dot{Q}_{S,k} = Q_g \frac{\partial c_{S,k}}{\partial t} \tag{6.11}$$

It has also been observed that the reaction kinetics of the degree of cure are temperature dependent. The temperature dependency of the rate of cure is defined using the model developed by Kamal and Sourour (1973):

$$\frac{\partial c_{S,k}}{\partial t} = f(c_{S,k}, T) = (d_1 + d_2 c_{S,k}^m)(1 - c_{S,k})^n \tag{6.12}$$

$$\text{where } d_1 = a_1 e^{-b_1/RT_k} \qquad d_2 = a_2 e^{-b_2/RT_k}$$

where a_1, a_2, b_1, b_2, m and n can be obtained by applying regression analysis to experimental data from DSC (differential scanning calorimetery) analysis for a given material. After experimentally determining the values for these parameters $\dot{Q}_S$, the rate of heat generation, can be redefined as follows:

$$\dot{Q}_{S,k} = Q_g(d_1 + d_2 c_{S,k}^m)(1 - c_{S,k})^n \tag{6.13}$$

To simplify the form of the energy equation, the following grouping parameter is defined:

$$\Omega = \frac{\lambda\, \Delta t}{c_p (h_S)^2} = a \frac{\Delta t}{(h_S)^2} \tag{6.14}$$

Substituting this grouping parameter into the energy equations puts this equation in the following tri-diagonal form:

$$-\Omega T_{S+1,k+1} + (2\Omega + 1) T_{S,k+1} - \Omega T_{S-1,k+1} = T_{S,k} + \frac{\Delta t}{\rho c_p} \dot{Q}_{S,k} \tag{6.15}$$

Example: four stress layers

The following equations exemplify the derivation of the governing equations for the energy transport, which can be solved at each time step for each element in the mesh to give the temperature at the finite difference point for a given stress layer. In this example for the sake of brevity only four stress layers are used. However, the method is the same for the case of more than four stress layers.

Equation 6.15 for the four stress layers becomes:

$$S = 1: \; -\Omega T_{0,k+1} + (2\Omega + 1) T_{1,k+1} - \Omega T_{2,k+1} = T_{1,k} + \frac{\Delta t}{\rho c_p} \dot{Q}_{1,k} \tag{6.16}$$

$$S = 2: \; -\Omega T_{1,k+1} + (2\Omega + 1) T_{2,k+1} - \Omega T_{3,k+1} = T_{2,k} + \frac{\Delta t}{\rho c_p} \dot{Q}_{2,k} \tag{6.17}$$

$$S = 3: \; -\Omega T_{2,k+1} + (2\Omega + 1) T_{3,k+1} - \Omega T_{4,k+1} = T_{3,k} + \frac{\Delta t}{\rho c_p} \dot{Q}_{3,k} \tag{6.18}$$

$$S = 4: \; -\Omega T_{3,k+1} + (2\Omega + 1) T_{4,k+1} - \Omega T_{5,k+1} = T_{4,k} + \frac{\Delta t}{\rho c_p} \dot{Q}_{4,k} \tag{6.19}$$

In the above equations $T_{0,k+1}$ and $T_{5,k+1}$ represent the distinct reference temperatures (the 'helper points'). One can then set the equations in the following matrix form, from which the desired temperatures $T_{1,k+1}$ to $T_{4,k+1}$ can be solved for in conjunction with the solution of the equation for the 'helper points' (defined further on in this section):

$$\begin{bmatrix} 2\Omega+1 & -\Omega & 0 & 0 \\ -\Omega & 2\Omega+1 & -\Omega & 0 \\ 0 & -\Omega & 2\Omega+1 & -\Omega \\ 0 & 0 & -\Omega & 2\Omega+1 \end{bmatrix} \begin{Bmatrix} T_{1,k+1} \\ T_{2,k+1} \\ T_{3,k+1} \\ T_{4,k+1} \end{Bmatrix} = \begin{Bmatrix} T_1^* + \Omega T_{0,k+1} \\ T_2^* \\ T_3^* \\ T_4^* + \Omega T_{5,k+1} \end{Bmatrix} \quad 6.20$$

where

$$T_1^* = T_{1,k} + \frac{\Delta t}{\rho c_p}\dot{Q}_{1,k} \qquad T_2^* = T_{2,k} + \frac{\Delta t}{\rho c_p}\dot{Q}_{2,k}$$

$$T_3^* = T_{3,k} + \frac{\Delta t}{\rho c_p}\dot{Q}_{3,k} \qquad T_4^* = T_{4,k} + \frac{\Delta t}{\rho c_p}\dot{Q}_{4,k}$$

The temperatures T_1^* to T_4^* represent the temperatures at the new time step in each of the respective four stress layers including the increase in temperature due to the reaction energy released during cure.

Energy transport after part ejection

EXPRESS also considers the heat transfer that occurs when the part is removed from the mould cavity and set aside to cool to ambient temperature. Additionally, upon ejection of the part warpage phenomena characteristic to the compression moulding process are accounted for by modifying the boundary conditions for the energy equations. The necessary modification to the above described one-dimensional heat transfer analysis is to modify the coefficient of thermal diffusion to reflect the transport of energy from the part to the cooler surroundings.

$$\alpha_O = \alpha_U = \alpha_{Air} \qquad \text{Coefficient of thermal diffusion (in still air)}$$
$$T_{WO} = T_{WU} = T_U \qquad \text{Temperature of the surroundings}$$

An energy balance on the upper edge of an element gives the temperature $T_{5,k+1}$ at the upper 'helper point' node (for the example where $n_S = 4$) as:

$$\dot{q} = \left(\frac{T_{n_S+1,k+1} + T_{n_S}^*}{2} - T_{wo}\right)\alpha_0 \equiv \left(T_{n_S}^* - \frac{T_{n_S+1,k+1} + T_{n_S}^*}{2}\right)\left(\frac{\lambda}{\frac{h_S}{2}}\right) \quad 6.21$$

where the following relation simply represents an interpolation between the node in the uppermost stress layer and the upper 'helper node', giving the temperature at the upper edge of an element:

$$\frac{T_{n_S+1,k+1} + T^*_{n_S}}{2} \tag{6.22}$$

Finally, one can solve the following expression for the temperature at the upper 'helper point' node:

$$T_{n_S+1.k+1} = T^*_{n_S}\left[\frac{\left(\frac{2\lambda}{\alpha_o h_S} - 1\right)}{\left(\frac{2\lambda}{\alpha_o h_S} + 1\right)} + \frac{2T_{wo}}{\left(\frac{2\lambda}{\alpha_o h_S} + 1\right)}\right] = T^*_{n_S} + \frac{2(T_{Wo} - T^*_{n_S})}{\left(\frac{2\lambda}{\alpha_o h_S} + 1\right)} \tag{6.23}$$

Following the same procedure for the bottom edge of the element one derives the following expression for the lower 'helper point' node:

$$T_{0,k+1} = T^*_1\left[\frac{\left(\frac{2\lambda}{\alpha_u h_S} - 1\right)}{\left(\frac{2\lambda}{\alpha_u h_S} + 1\right)} + \frac{2T_{wu}}{\left(\frac{2\lambda}{\alpha_u h_S} + 1\right)}\right] = T^*_1 + \frac{2(T_{Wu} - T^*_1)}{\left(\frac{2\lambda}{\alpha_u h_S} + 1\right)} \tag{6.24}$$

6.2.3 Calculation of fibre orientation

The simulation of the fibre orientation during the compression moulding simulation is essential for an accurate prediction of the thermomechanical behaviour and the final mechanical properties of complex, fibre-reinforced parts. The fibre orientation is influenced by the flow of the material (Fig. 6.4). For this reason a process simulation has to calculate the orientations and redistribution of the fibre reinforcement from the very beginning of the process until the end of the filling stage. Additionally the ability to define any charge pre-orientation that might have developed during the processing of the mat or bulk charge is necessary. The following section provides an overview of the models and theory, which make up the foundation of the fibre orientation simulation.

The fibre orientation distribution is described with an angle class system. Figure 6.5 shows how the distribution function is discretised into various angle classes. These angle classes are defined with respect to a local coordinate system for each element. The various class discretisation acts as the foundation upon which the fibre orientation function can be calculated. At the bottom half of Fig. 6.5, two examples of the distribution function can be seen. The distribution on the left-hand side shows an isotropic fibre distribution, while that on the right-hand side displays an anisotropic fibre distribution where the main fibre orientation direction occurs at 90º. Another method to describe the fibre orientation is the use of orientation tensors.

The consideration of fibre transport

Due to the flow process, the fibres not only rotate but are also transported beyond the element boundaries. This demands that both a different fibre

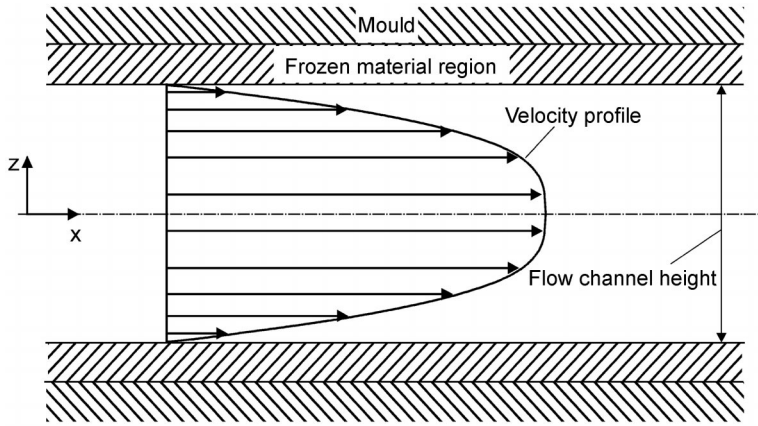

6.4 Velocity profile in the through-thickness direction.

orientation as well as different fibre volume content must be recorded in a given element at each time step. It is therefore necessary to access the fibre orientation and fibre volume content of the neighbouring elements to satisfy the continuity conditions. Therefore the average flow rate for each element over all of the layers is calculated. The distribution function for each of the neighbouring elements is then weighted for each layer and added to the previous distribution function for the corresponding layer. Figure 6.6 clarifies the transfer of material and the corresponding orientation between two neighbouring elements. The value of the fibre distribution function must be converted from the local fibre angle coordinate system used in element A to that used in element B.

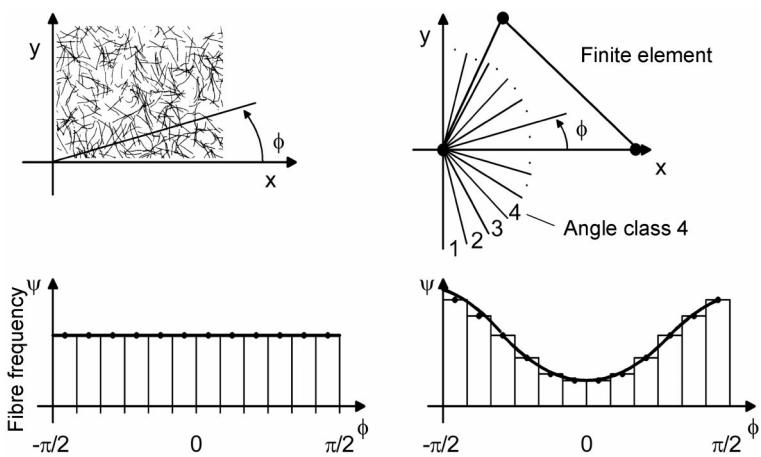

6.5 Finite element and the angle class system.

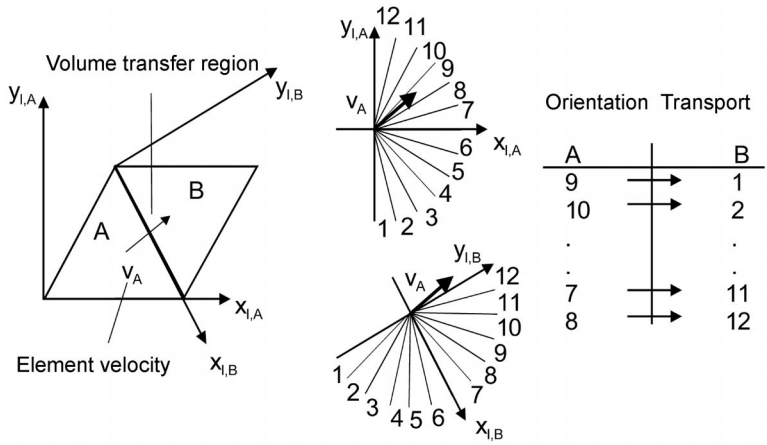

6.6 Fibre orientation transport between elements.

Model for calculation of fibre rotation

The first notable attempt to model the fibre orientation in composite parts was developed by Jeffery (1922). The model uses two equations to describe the three-dimensional rotation of a single ellipsoid in a high viscous Newtonian matrix. The rotation of the ellipsoid results from the difference in velocity at its ends. An important prerequisite for the validity of this model is that the matrix has a lower fibre concentration than the critical fibre concentration, while Jeffery's model does not account for fibre-fibre interaction. The critical fibre concentration describes the point at which an individual fibre is no longer oriented solely as a result of the varying velocity field, but whose orientation is also influenced by the presence of neighbouring fibres. The critical fibre concentration is defined to be 1% of the total part volume. Equation 6.25 describes the rotation of a fibre for the 2-dimensional case in which all of the fibres lie in a single plane, where r_e represents the axis length ratio and $v_{x,x}\ldots$ represent the velocity distributions respective to the various flow directions (Advani 1987).

$$\frac{\partial \phi}{\partial t} = \frac{r_e^2}{r_e^2+1}\left(\sin\phi\cos\phi(v_{y,y}-v_{x,x}) + \cos^2\phi v_{y,x} - \sin^2\phi v_{x,y}\right) - \frac{1}{R_e^2+1}\left(\sin\phi\cos\phi(v_{y,y}-v_{x,x}) - \sin^2\phi v_{y,x} + \cos^2\phi v_{x,y}\right) \qquad 6.25$$

For fibre reinforced materials with a fibre volume fraction of more than 1% (usually the case) the preferred model becomes the Folgar-Tucker model (Folgar 1983, Folgar and Tucker 1984). This model is based on Jeffery's model, but includes the consideration of interaction between the individual fibres, thereby ensuring that the fibres cannot become oriented 100% in any direction.

Although the Folgar-Tucker fibre orientation model is much more flexible

than the aforementioned Jeffery model, and therefore, more applicable for complex parts, it has its disadvantages. Namely, to produce a solution with stable results, the equation that describes the fibre rotation needs the help of an additional numerical procedure. Furthermore, the use of this model requires the ability to access required input parameters from the flow simulation in order to solve the governing fibre orientation equation (i.e. the description of the shear and extensional velocities in the flow field).

The following assumptions were made in the derivation of this model (Folgar 1983, Folgar and Tucker 1984):

1. The fibres can be considered as rigid bodies with a uniform length and diameter.
2. The fibres are much larger than the molecules of the surrounding material such that the effect of Brownian motion can be negated.
3. The fibre-matrix compound is incompressible.
4. The viscosity of the material matrix is so high that inertial effects can be negated.
5. The fibres are randomly distributed throughout the matrix material.
6. There are no externally applied forces or moments on the fibres.
7. Interaction between two fibres takes place when the centres of gravity of these fibres move past one another within a distance that is smaller than the length of the fibres.
8. All of the interactions between the fibres are irreversible and statistically evenly distributed. Each interaction causes a modification of the fibre angle, which is independent of the current orientation angle of the fibre.

Because it is not practical to consider each single fibre interaction separately for complex geometries, Folgar and Tucker considered the fibre orientation using a statistical approximation applicable to the entire domain. This statistical approximation, the fibre distribution function ψ, corresponds to a Gaussian probability distribution of the fibre orientation. This function must satisfy the following continuity equation, which encompasses all of the fibres rotating into and out of an arbitrary control volume within the flow field:

$$\frac{d\psi}{dt} = \frac{\partial \psi}{\partial t} + v_x \frac{\partial \psi}{\partial x} + v_y \frac{\partial \psi}{\partial y} = -\frac{\partial (\psi \dot{\phi})}{\partial \phi} \tag{6.26}$$

The above equation is simplified as the material convection terms drop out with reference to a stationary coordinate system.

Folgar and Tucker extended Jeffery's equation for the rotational speed of a single fibre with the addition of a dampening term (eq. 6.27).

$$\begin{aligned} \frac{\partial \phi}{\partial t} = & -C_I \dot{\gamma} \frac{1}{\psi} \frac{\partial \psi}{\partial \phi} - \sin\phi \cos\phi \, v_{x,x} \\ & - \sin^2\phi \, v_{x,y} + \cos^2\phi \, v_{y,x} + \sin\phi \cos\phi \, v_{y,y} \end{aligned} \tag{6.27}$$

In the above equation, the variable $\dot{\gamma}$ represents the second invariant of the rate of deformation tensor (eq. 6.28), and C_I represents the fibre interaction coefficient that acts as a material parameter to describe the material orientation behaviour.

$$\dot{\gamma} = \sqrt{2v_{x,x}^2 + (v_{x,y} + v_{y,x})^2 + 2v_{y,y}^2} \qquad 6.28$$

The frequency of the fibre-fibre interaction is described within the model proportional to $\dot{\gamma}$.

Equations 6.26 and 6.27 lead to the following differential equation (eq. 6.29) describing the time dependency of the fibre orientation function as a function of the fibre interaction coefficient ψ, as well as the shear and extensional velocities present within the flow field.

$$\frac{\partial \psi}{\partial t} = C_I \dot{\gamma} \frac{\partial^2 \psi}{\partial \phi^2} - \frac{\partial}{\partial \phi} \begin{bmatrix} \psi(-\sin\phi\cos\phi\, v_{x,x} - \sin^2\phi\, v_{x,y} + \\ +\cos^2\phi\, v_{y,x} + \sin\phi\cos\phi\, v_{y,y} \end{bmatrix} \qquad 6.29$$

The following section briefly discusses the validity of the assumptions made to derive the above equation with respect to the compression moulding of fibre-reinforced parts. The consideration of the fibres as rigid bodies within compression moulding materials is a reasonable assumption. One could argue that the presence of very long fibre filaments or bundles may deviate from the rigid body assumption. In this case it has been shown that one can also consider a long fibre as smaller, broken off, inflexible fibres, linked together one after the other (Diest 1996). The assumption that Brownian motion can be negated is valid for the considered material since the relative fibre size is much larger than the size of the matrix molecules.

The third and fourth assumptions have been validated many times in various studies in the field of rheological theory (Heber 1995, Michaeli 1990). The random distribution of the fibres in a material matrix, along with the assumption of a z-symmetric velocity profile, implies that the volume of fibres remains constant above and below the thickness half-plane of the part and that no mixing occurs between these two regions during the flow process. This assumption is no longer valid for complex geometries involving significant material flow in all three coordinate directions. The sixth assumption that no external forces are applied is appropriate under the consideration that external forces can only develop along the mating edges of the mould. When the charge positioning is done carefully, such that the majority of the flow front reaches these edges at approximately the same time, the influence of these external forces on the flow can be overlooked.

The seventh and eighth assumptions having to do with the fibre interaction are the core assumptions made for this model. Folgar (1983) and Folgar and Tucker (1984) show that these assumptions have been confirmed in many different experimental works with fibre-reinforced, thermoset compression moulding

materials. A translation of these results for thermoplastic materials is found in Semmler (1998). The consideration of the thermoplastic specific properties (e.g., discrete layer fibre orientation) will be mentioned later in this chapter.

Solution of the differential equation

Because the differential equation for the calculation of fibre rotation (eq. 6.29) is not solvable using analytical methods, numerical methods must be employed that are both computationally stable and efficient. Therefore, the governing equations for the fibre orientation must be discretised and rewritten in implicit form.

The implicit method requires that the value of the function for the current time step is ascertained from the value of the function of the neighbouring nodes at the current time step (Fig. 6.7, left side). This also means that the solution of the corresponding finite difference equation cannot be attained without the use of an explicit finite differencing method at the boundary values (angle classes 1 and 25) (Fig. 6.7, right side).

In order to make use of the implicit method, eq. 6.29 must first be rewritten in the following form:

$$\begin{aligned}\frac{\partial \psi}{\partial t} &= C_I \dot{\gamma} \frac{\partial^2 \psi}{\partial \phi^2} \\ &- \frac{\partial \psi}{\partial \phi}(\sin\phi\cos\phi(v_{y,y} - v_{x,x}) - \sin^2\phi\, v_{x,y} + \cos^2\phi\, v_{y,x}) \\ &- \psi \frac{\partial(\sin\phi\cos\phi(v_{y,y} - v_{x,x}) - \sin^2\phi\, v_{x,y} + \cos^2\phi\, v_{y,x})}{\partial\phi}\end{aligned} \qquad 6.30$$

To put this equation into an implicit form, the substitutions outlined in eqs. 6.31–6.34 are made in eq. 6.30.

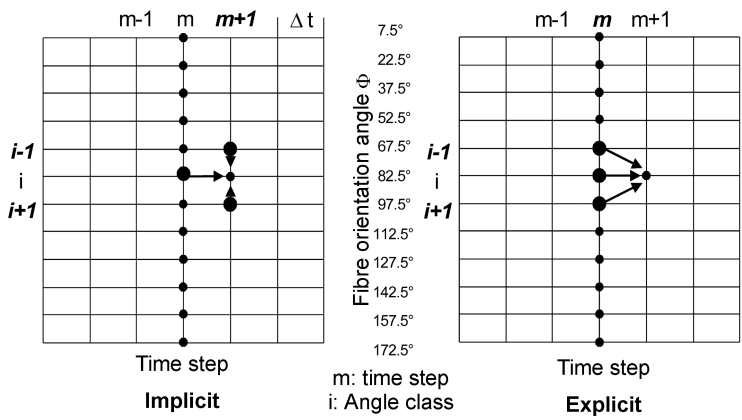

6.7 Implicit and explicit finite element methods.

$$\psi = \psi_i^{m+1} \tag{6.31}$$

$$\frac{\partial \psi}{\partial t} = \frac{\psi_i^{m+1} - \psi_i^m}{\Delta t} \tag{6.32}$$

$$\frac{\partial \psi}{\partial \phi} = \frac{\psi_{i+1}^{m+1} - \psi_{i-1}^{m+1}}{2\Delta\phi} \tag{6.33}$$

$$\frac{\partial^2 \psi}{\partial \phi^2} = \frac{\psi_{i+1}^{m+1} - 2\psi_i^{m+1} + \psi_{i-1}^{m+1}}{\Delta\phi^2} \tag{6.34}$$

The resulting finite difference equation is solved for ψ_i^{m+1}, converted into tri-diagonal form, the boundary conditions are explicitly defined, and the system of equations is solved by using a Gaussian-based matrix solving algorithm (Schwarz 1986).

Thermoplastic discrete layer calculation of the fibre orientation

The calculation of the fibre rotation and transport for thermoplastic materials must be approached using discrete layers. Dividing the geometry into layers allows consideration of the difference in the velocity profile with respect to the flow channel height as well as the effect of the transient flow channel height due to the cooling and eventual freezing of the material. Figure 6.4 schematically displays a typical velocity profile during the compression moulding of a thermoplastic material and shows that the fibres become fixed in the regions close to the mould walls as the material freezes. Figure 6.8 shows the principle applied to ascertain the orientation using a discretisation of layers. One can see from this figure that two different layer discretisations are used. The variable layers are allowed to change their respective thickness and position during the process, whereas the stationary layers maintain the same thickness and position throughout the process.

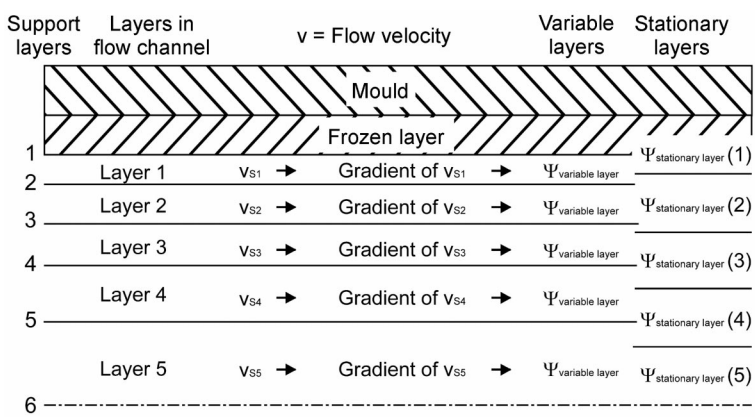

6.8 Layer discrete fibre orientation.

In comparison to the middle of the flow channel, the velocity profile gradient is clearly higher in the regions closer to the mould walls (see Fig. 6.4). For this reason, a finer discretisation of the variable layers is applied closer to the mould walls. The thickness of the variable layers and their respective positions are dependent upon the height of the flow channel (which varies during the filling stage; a major difference between modelling compression moulding in comparison to injection moulding), as well as the thickness of the layer that is considered to be completely frozen.

The fluid velocity for the variable layers is calculated from the shear velocity present for a given layer as follows:

$$v_\mu = \dot{\gamma}\, h_{vS} + v_{\mu+1} \qquad 6.35$$

Interpolation is used to obtain the average velocity located at the middle of each variable layer for every element. The velocities at the respective nodes for an element are then calculated using the weighted system based on the element area, from which the gradients at the element centre can be ascertained through differentiation.

These gradients are used as the input parameters for eq. 6.29, the computation of the fibre orientation. For each time step, the corresponding distribution function, whose value is dependent upon the current position and thickness of the frozen layers, is averaged and saved in each of the five static layers. These stationary layers, defined at the beginning of the computation, have a tenth the thickness of the part, and their positions remains constant during the entire process. At the end of the flow process, the fibre orientation in both the melt and frozen material is saved in the stationary layers, which can then be accessed in displaying the final orientation of the part.

The consideration of fibre pre-orientation

As a result of the process used in the production of fibre-reinforced materials for compression moulding, these materials contain a fibre pre-orientation, even before the compressing moulding process begins. For example, pre-orientation originates in the production of the fibre mat for SMC/mat-GMT materials (where the fibres tend to become oriented in the machine direction for mat-weave lay-ups), as well as in the plastification process of bulk materials as a result of the screw geometry. In the past, these material characteristics, as well as the definition of charge positions, were usually ignored in the design process. However, practical investigation into the influence of pre-orientation of charges and their positioning show these variables can strongly influence the mechanical and thermo-mechanical properties of the part. The corresponding algorithm for considering fibre pre-orientation is outlined in Fig. 6.9.

Like the fibre orientation, the pre-orientation is defined using a distribution factor. The main direction of the orientation as well as the position of the

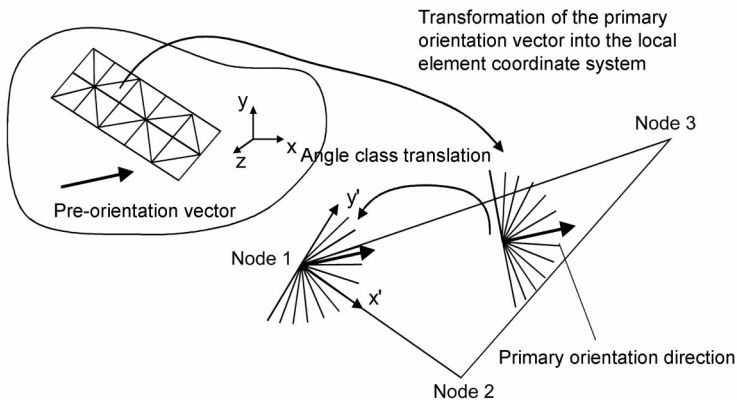

6.9 Translation of fibre orientation.

charges must also be defined. The positioning of the charges is accomplished by selecting certain elements of the geometry mesh and defining them as a group. The main orientation vector is converted from global into element local coordinates at the beginning of the calculation. Finally, the distribution function, as shown in Fig. 6.9 containing 25 discrete angle classes, is converted into the local element angle class system.

The pre-orientation distribution factor is defined as a material parameter, which requires that the distribution is measured for each charge. This measurement is most easily obtained using a program, which can calculate the fibre orientation from digitised images of actual charges (e.g., FiberScan).

6.3 Examples of use of the simulation

In the following some examples should show the capabilities of the simulation. At first a non-isothermal simulation of the flow fronts is presented that helps the user to detect weld lines and non filled areas due to a too early freezing of the material. Based on this simulation the fibre orientation simulation could be done that enables a stiffness and failure analysis of long fibre reinforced parts. Last but not least the simulation can help to build up an easy quality control system that is based on the calculation of the centre of force. All the process simulations were done with the simulation program EXPRESS, developed by the Institute of Plastics Processing (IKV), Aachen, Germany in cooperation with M-Base Engineering and Software GmbH, Aachen. The mechanical simulations were done by the finite element program Abaqus.

6.3.1 Flow simulation

The flow simulation results of three geometries are shown: the first one is a door panel made out of SMC which is a rather shell-like part with very high

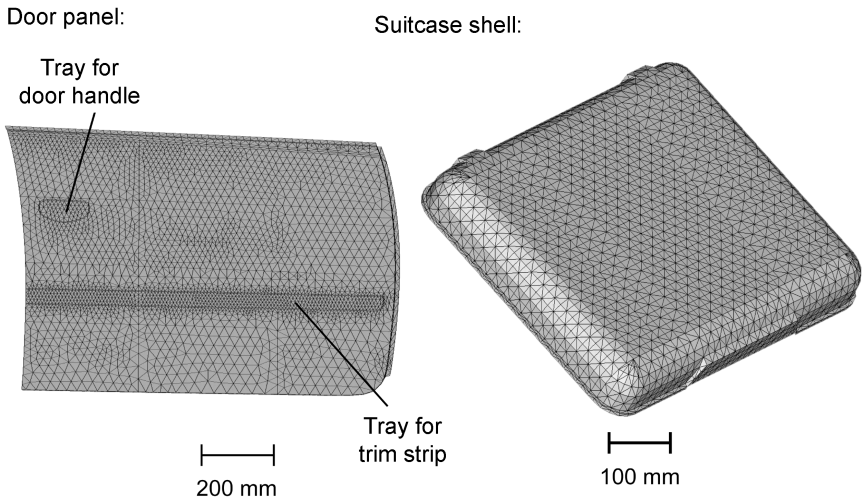

6.10 Example geometries (I): door panel and suitcase shell.

requirements on the surface quality. The second one is a suitcase shell made out of GMT. The third one is a dashboard made out of long fibre reinforced thermoplastics (LFT) in the long fibre extrusion compression moulding (ECM) process, which should show, that rather complex parts with undercuts could be simulated, too. These parts are shown in Figs 6.10 and 6.11.

Figure 6.12 shows the calculated flow fronts for the door panel in comparison to short shots that were made in the compression moulding process. The dark grey area represents the calculated flow front and the coloured lines represent the measured flow fronts. For these measurements the closing process was stopped at a defined stroke. With these short shots one gets

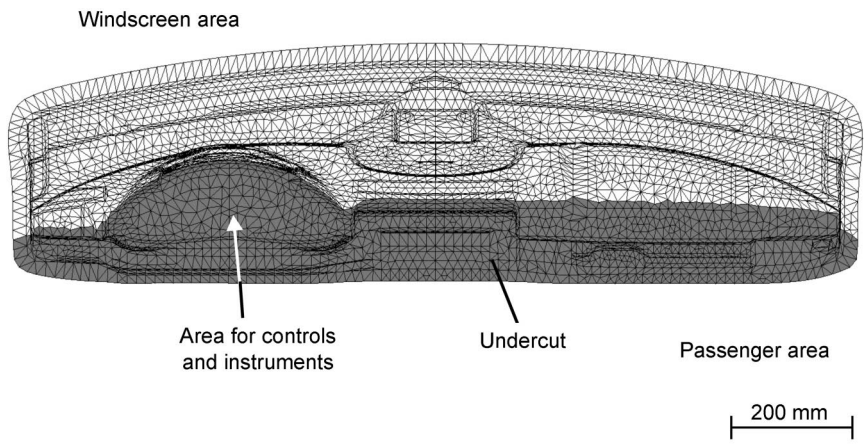

6.11 Example geometries (II): dashboard.

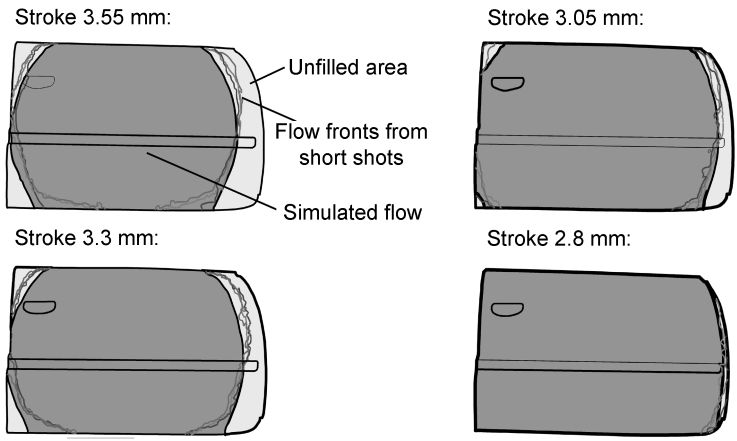

6.12 Comparison of the flow front with short shots.

unfilled parts representing the flow front at the stopped stroke. Figure 6.12 shows that there is a certain deviation of the flow fronts measured in three different tests where the closing process was stopped at the same stroke. This may come from the variation in the process, e.g. charge size or charge position. However, the calculated flow of the material is in good accordance with the measurements.

Beneath the flow fronts the calculated press force is a very important process parameter, because with its knowledge one can estimate whether the existing presses can be used to manufacture new parts or if a new investment is necessary. Figure 6.13 shows the measured press force for the suitcase shell made out of GMT in comparison to the calculated press force for a non-isothermal

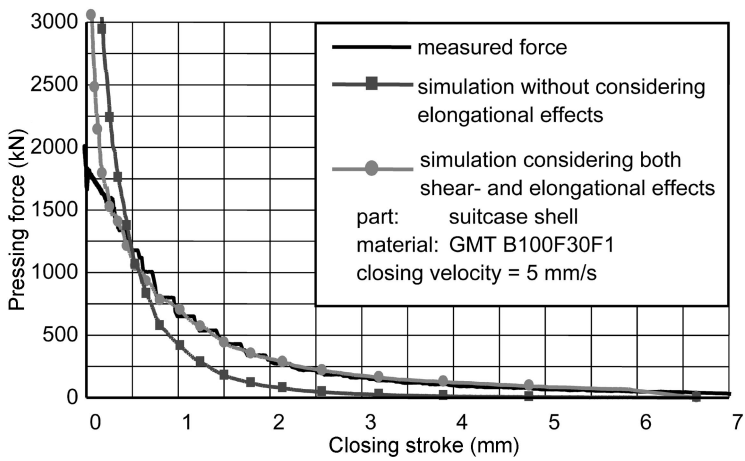

6.13 Comparison of the calculated pressing force with measurements (material: GMT).

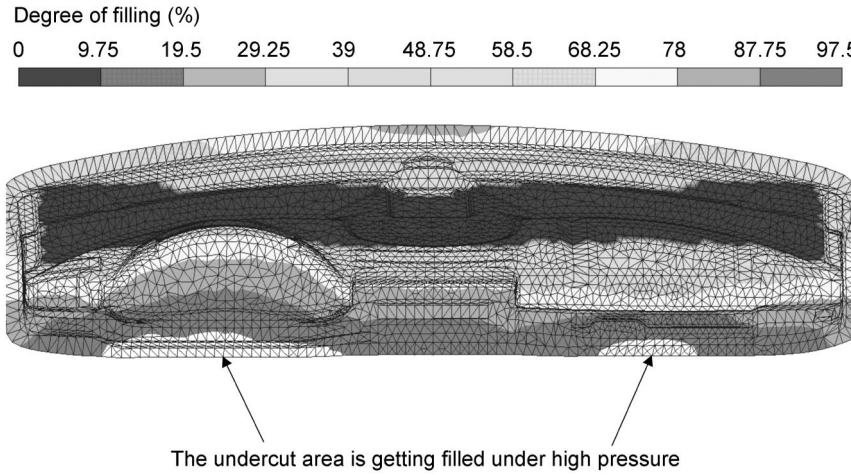

6.14 Flow fronts at the end of the filling process.

compression moulding process. The calculation was done first with the assumption of a pure shear flow without wall slippage and additionally an advanced simulation under consideration of both strain effects and wall slippage was done. The result shows that for both simulations the calculation agrees sufficiently on the measured data. Furthermore, the advanced simulation considering the strain flow of the material is more precise. The results show clearly that the process simulation is able to predict the press force for the non-isothermal compression moulding process of long fibre reinforced thermoplastics.

Usually there are not just parts having a shell-like geometry. In Fig. 6.14 the calculated flow front of a thermoplastic dashboard is shown. This is a very complex part with undercuts as shown in Fig. 6.11. Nevertheless a simulation is possible.

6.3.2 Fibre orientation simulation

The fibre orientation simulation is very useful to detect areas with a very high fibre orientation in the part. These areas do usually have very poor mechanical properties perpendicular to the fibre orientation and they tend to high warpage due to the different thermo-mechanical properties in and perpendicular to the fibre orientation. Additionally, with the knowledge of the local fibre orientation distribution a prediction of the local anisotropic material behaviour is possible.

For this example the door panel was used (Fig. 6.10). In order to assess the possibilities of the simulation three different charge positions were defined to get different local fibre orientation distributions. The calculation was verified with experiments where the fibre orientation was measured by analysing x-ray

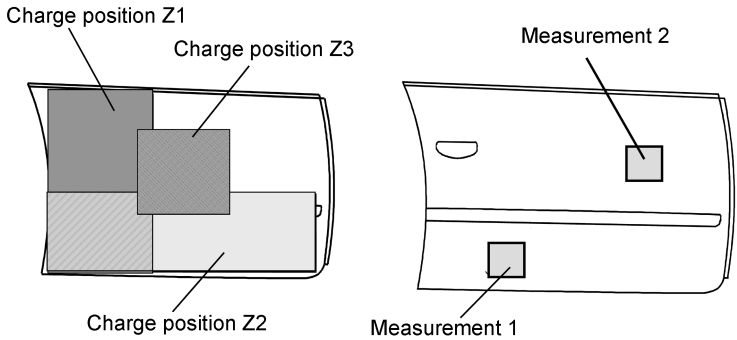

6.15 Positions of the charge and measurement of the fibre orientation distribution.

pictures with the image processing software FibreScan. The charge positions and the location where the orientation was measured are shown in Fig. 6.15. Figure 6.16 shows the calculated fibre orientation distributions in comparison with measurements for both positions. The diagram shows a clear accordance of the simulated orientations with the measurements. Thus a prediction of the fibre orientation is possible for shell-type parts made out of SMC. This also leads to very good simulation results of the calculation of the mechanical part properties as shown below.

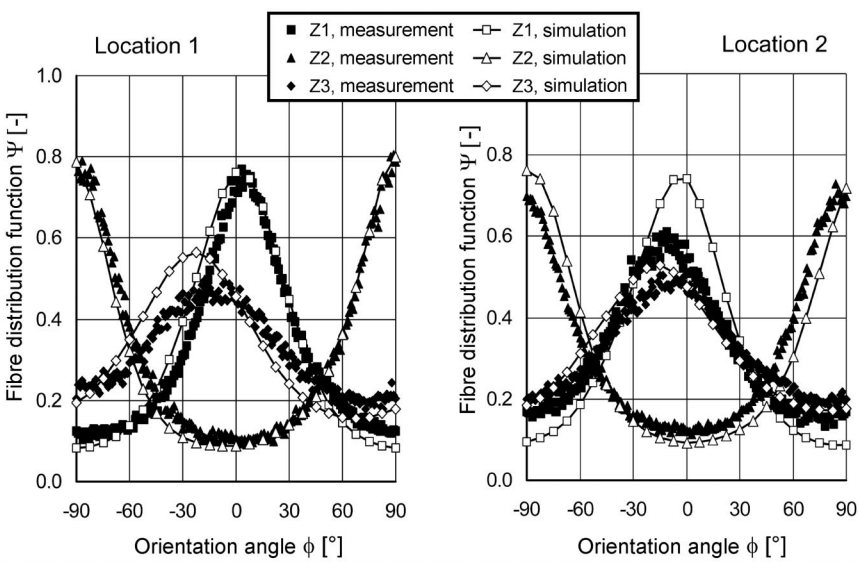

6.16 Comparison of the calculated fibre orientation with measurements.

6.3.3 Stiffness and failure analysis

This section briefly describes the basic composite theory to archive a calculation of the local material properties at each point of the component using initial numbers for the matrix and fibre properties. The combination of micro- and macromechanical theory simplifies the analysis process without performing any mechanical testing. These models require the calculated fibre orientation. This calculation process runs in two stages as outlined in Fig. 6.17. In the first step a micromechanical model is applied to determine the anisotropic stiffness parameters for one layer. This model assumes unidirectional fibres parallel and perpendicular to the principal orientation of the material.

The laminate theory is then applied to calculate the element stiffness properties accumulating the stiffness from all layers in the element regarding the differing directions of the principal orientation in each layer. The thickness of a single layer corresponds to the value of a particular angle class from the fibre distribution function and takes on the same directional alignment. The model effectively combines the individual layers using the values determined from the micromechanical model for each individual laminate layer and their respective alignments, giving the resultant elasticity tensor for an element.

Micromechanical model

With the application of a micromechanical model one can calculate the fibre-matrix material properties by separately considering the material as being constructed from unidirectionally oriented fibres and a matrix material. Halpin and Tsai developed the micromechanical model for unidirectional fibre reinforced materials. However, the components produced in compression

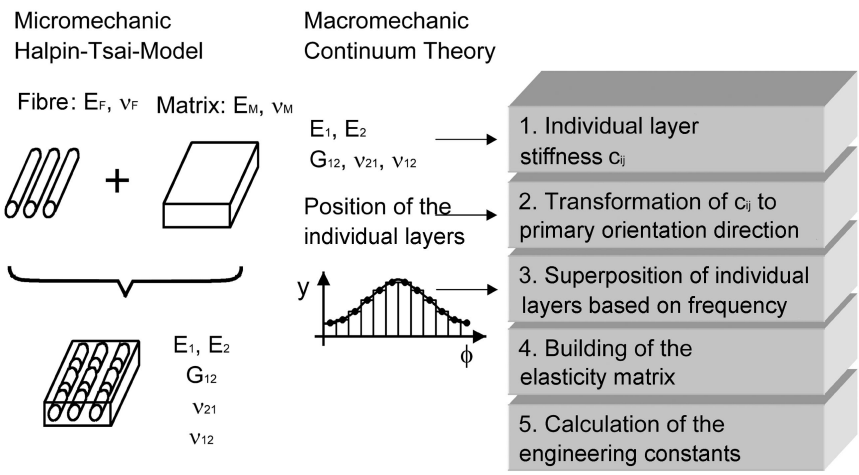

6.17 Calculating the engineering constants.

moulding are not oriented unidirectionally. Therefore, 25 different layers are assumed each having a slightly different principal orientation.

Using eqs. 6.36–6.41, the elastic moduli, shear moduli and Poisson's ratios are calculated for a single orientation angle 'layer' using the following relationships:

$$E_1 = E_M \frac{1 + \xi\kappa\Phi}{1 - \kappa\Phi} \quad \text{where} \quad \xi = 2\frac{l_F}{d_F} \tag{6.36}$$

$$E_2 = E_M \frac{1 + \xi\kappa\Phi}{1 - \kappa\Phi} \quad \text{where} \quad \xi = 2 \tag{6.37}$$

$$\kappa = \frac{\frac{E_F}{E_M} - 1}{\frac{E_F}{E_M} + \xi} \tag{6.38}$$

$$\nu_{21} = \nu_F\Phi + \nu_M(1 - \Phi) \tag{6.39}$$

$$\nu_{12} = \nu_{21}\frac{E_2}{E_1} \tag{6.40}$$

$$G_{12} = G_M \frac{1 + \xi 0.5\Phi}{1 - 0.5\Phi} \quad \text{where} \quad \xi = 1 \tag{6.41}$$

Macromechanical model

These 25 layers are then combined using the principle of superposition to calculate the anisotropic material stiffness for each element (or each stress layer of each element). This method is known as the Continuum Theory, developed by Puck and Halpin (Puck 1967). The specific thickness for a given imaginary layer is defined using the value of the probability parameter, which is determined from the fibre distribution function. In this way, the influence of the fibre orientation of a continuous material is transformed into a calculation for a laminate material composed of 25 layers with unidirectional material properties. The combination of the micro- and macromechanical models leads to the numerical calculation of the composite material properties. In the following section, models for the above material properties are introduced to show how the temperature and pressure dependency of these properties can also be included in the calculation of the final composite properties.

For a failure analysis a global failure criterion is used. It evaluates within the analysis whether the current stress state causes a failure or not. Up to now, distinct failure modes for fibre fracture and inter fibre fracture have not been available for long fibre reinforced plastics. The used global failure criterion (eq. 6.42) describes the failure factor f_E with a polynominal formulation such as the Norris criterion (Echaabi *et al.* 1996). If this factor is equal or larger than 1 failure of the material is calculated.

$$f_E = \left(\frac{\sigma_1}{R_1}\right)^2 + \left(\frac{\sigma_2}{R_2}\right)^2 + \left(\frac{\sigma_1\sigma_2}{R_1R_2}\right)^2 + \left(\frac{\tau_{21}}{R_{21}}\right)^2 \quad 6.42$$

The parameters R of this equation are the tensile and the compression strength in principal fibre orientation and perpendicular to it as well as the shear strength. The different strength values depend on the fibre orientation distribution and thus they are locally different and have to be measured for different fibre volume content and orientation degrees (Piry 2004).

Example of mechanical simulation

To show the possibilities of the coupled flow and mechanical simulation an analysis of the door panel mentioned above was done. For the mechanical simulations the charge positions Z1 and Z2 (Fig. 6.15) were assumed. With the given numbers of the local fibre orientation distribution and fibre content the local anisotropic material data was calculated. To prove the calculations a mechanical, linear distributed load of 200 Newtons was assumed. The calculated deformations of the part were compared to measurements. The test set up is shown in Fig. 6.18. The comparison shows, that the stiffness analysis of SMC parts closed to experiment (Fig. 6.19). In order to check the influence of the fibre orientation on the local stiffness the deformation along the section A-A drawn in the figure was analysed in more detail. Figure 6.20 shows the comparison of three calculations with different assumptions of the material behaviour with the measurements. The isotropic calculation shows a big deviation of the calculated deformation to the measurement in opposition to calculation with the assumption of anisotropic material behaviour. However, the difference between the linear calculation and the more complex calculation with the assumption of a non-linear material behaviour is very small in the stiffness analysis. This changes in the failure analysis. Here the failure was defined with the start of surface cracks. Figure 6.21 shows the calculated failure factor of the linear and the non-linear calculation along the section A-A. The charge position for this analysis was position Z1. Here a failure factor greater than 1 assumes the appearance of surface cracks in the area. Additionally the area where these surface cracks were detected on the section is shown in the figure. It is shown that the more complex simulation of the mechanical properties leads to a better

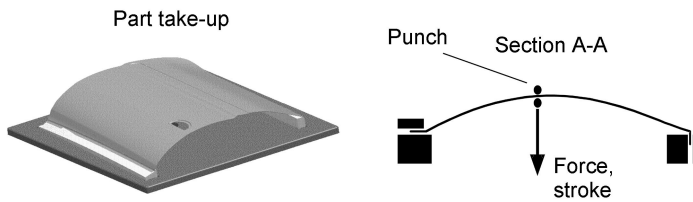

6.18 Set up of the mechanical tests.

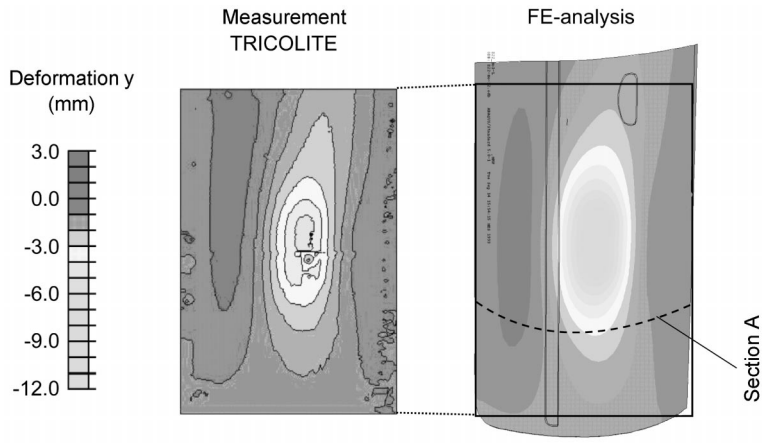

6.19 Comparison TRICOLITE-measurement and FE-analysis (Z2, $F = 200$ N).

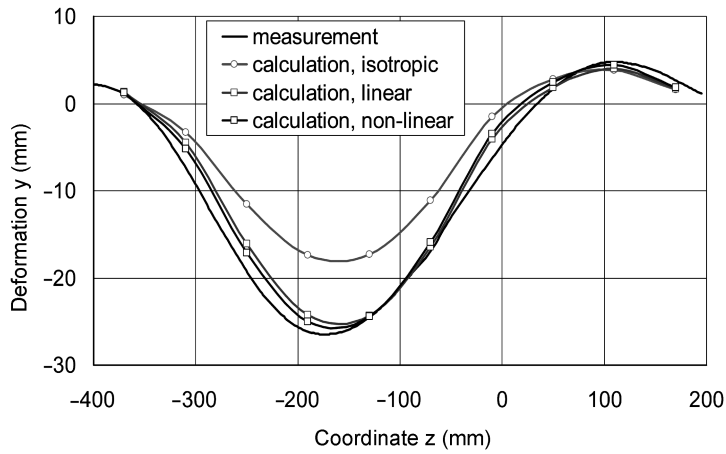

6.20 Comparison measurement and FE-analysis (blank Z1, section A).

prediction of the failure behaviour and gives the part designer the opportunity to tap the whole material potential. On the other hand, the non-linear simulation is much more complex and needs higher efforts to measure the material data.

6.3.4 Quality control

Process simulation programs are opening up new possibilities in quality assurance. By using process simulation one can determine and visualise process data (e.g., local pressures, temperatures, velocities, etc.) on the whole part. With this knowledge the sensor position can be optimised in order to measure the process data at the critical spots.

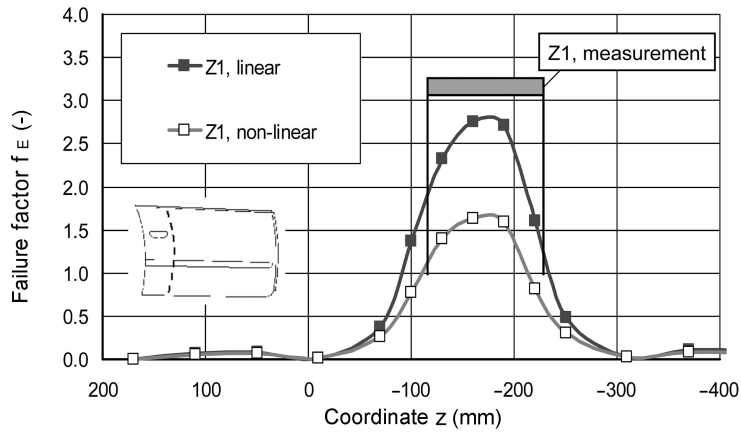

6.21 Failure factor f_E for crack failure.

The most important parameters that can be measured on the press without the sensors in the mould are: press force, press work, forces of parallelism, cylinder press stroke and closing velocity. One easy value that characterises the moulding process is the time dependent behaviour of the centre of force.

From the four forces of the parallelism cylinders $F_{Parallel}$ one can calculate a resultant force F_{Res} (Fig. 6.22). The vectorial change of this resultant force regarding the centre of gravity of the mould describes the flow of the material. Thus, this is an easy method to monitor several process parameters like charge position, charge size, closing velocity, etc. A compressed form of this description is the norm of the vector. This can be easily calculated and monitored by the data logging of the press.

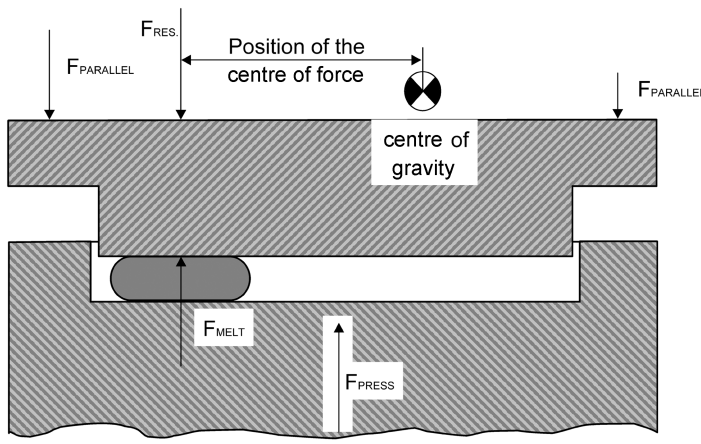

6.22 Determining the center of force.

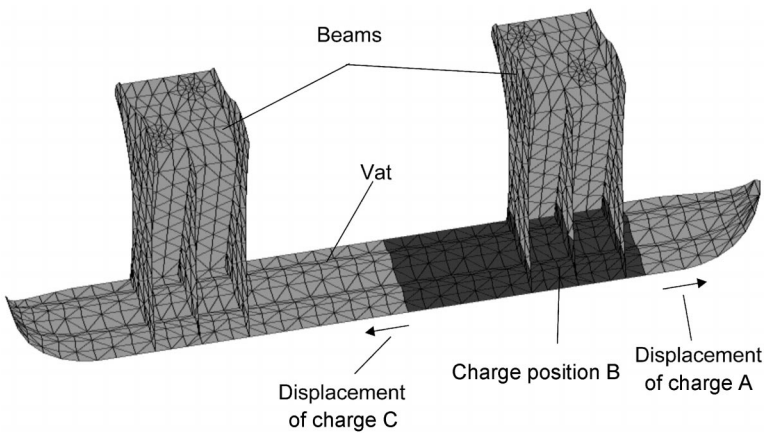

6.23 Charge positions for the sled runner.

Additionally it can be computed by simulation in order to get target data and to define specific setpoint values for the centre of force. Practical studies were carried out for a sled runner manufactured on a parallelism-controlled 2000 kN press. In these studies the charge position on the vat differs by 10 mm (Fig. 6.23). Figure 6.24 shows the variation of the centre of force for different charges, with different positions in the cavity. The deviation of the curve with different blank positions comes out very clearly. The results from a process simulation with charge position B is in good agreement with the corresponding measurements. The other parts made with charge positions A and C do not meet the required tolerances for charge position. This example shows that with the aid of process simulation software the manufacturer is able to derive set point values for a quality control system, which is the basis for a part assessment.

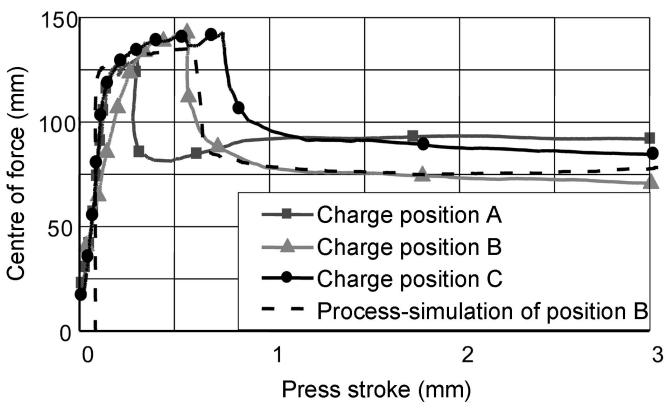

6.24 Influence of the charge position on the centre of force.

6.4 Measurement of the material data

Unfortunately, there is a wide variety of possible mistakes that could lead to incorrect results of the simulation. Besides the assumptions of wrong process parameters or bugs in the simulation software the assumption of suboptimal material data is a reason for incorrect results. Therefore the user has to keep in mind that without good material data one could not achieve the full potential of the simulation. One of the key material parameters is viscosity. A screening analysis on the deformation energy, which is the integral of the press force, shows that the viscosity parameters have a major influence on the calculated pressing force (Fig. 6.25). The viscosity of long fibre reinforced materials could be measured with special rheometer types called squeeze flow rheometers. One type of squeeze flow rheometer is the Press rheometer developed by Oelgarth (1997). The Press rheometer is a small mould with an open shear edge where the material can be withdrawn during the closing procedure. The set up of the rheometer is shown in Fig. 6.26. During different isothermal compressions, each with different temperatures and closing speeds, the press forces were measured. An analytical model is able to calculate the progression of the press force for this rather easy flow. Thus the viscosity parameters, which are a part of the analytical model, were determined by a non-linear regression analysis of these force progressions (Fig. 6.27). A detailed description of the proceeding is shown in (Oelgarth 1997, Ritter 2003). Alternative concepts for viscosity measurements are shown in (Bush *et al.* 2000, Orgeas *et al.* 2001).

The result of the measurement continues to improve, if one evaluates the measurement under consideration of the wall slip effect at the mould surfaces.

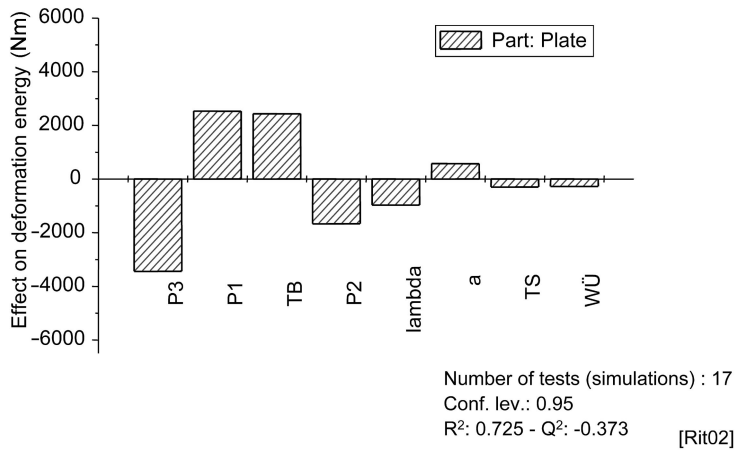

6.25 Influence of the material parameters on the deformation energy (thermoset material).

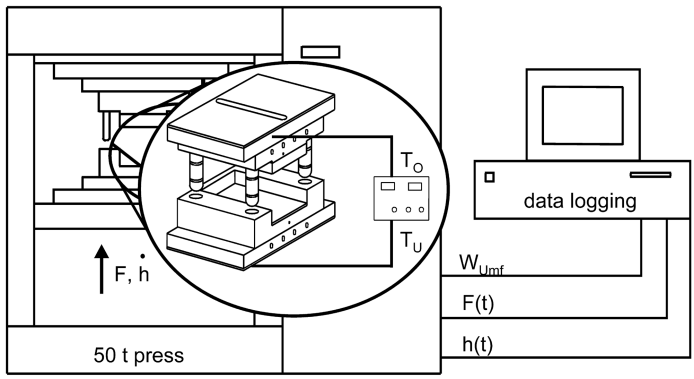

6.26 Set up of the press rheometer Rheopress.

Figure 6.27 shows the measured forces for a SMC and the fitted curves with and without consideration of the wall slip effects (Ritter 2003, Schmachtenberg and Skrodolies 2005). Figure 6.28 shows clearly that the fitted curves under consideration of wall slip effects deviate much less from the measured data than the fitted curve with the assumption of wall stick behaviour even by the analysis of the isothermal compression of thermoplastics. With this developed procedure it is possible to determine the viscosity parameters as well as wall slip coefficients.

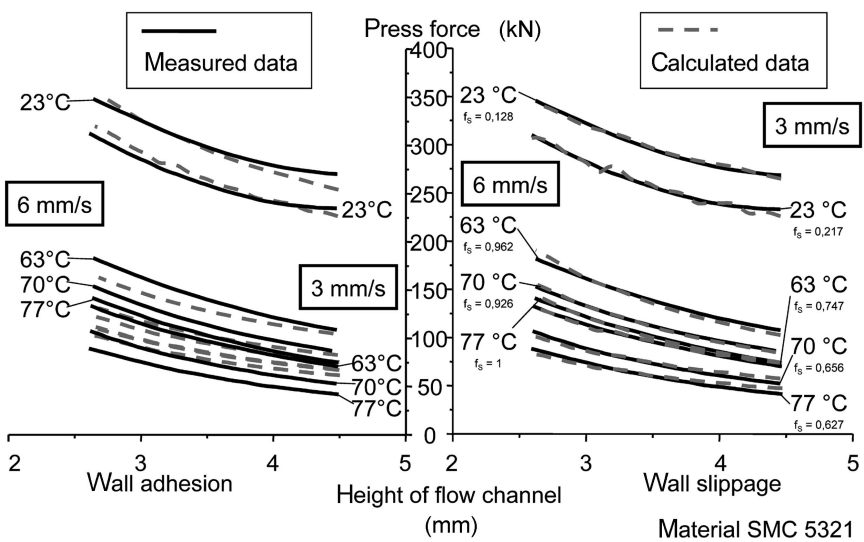

6.27 Press rheometer analysis: comparison of the analysis with wall adhesion and wall slippage effects (SMC).

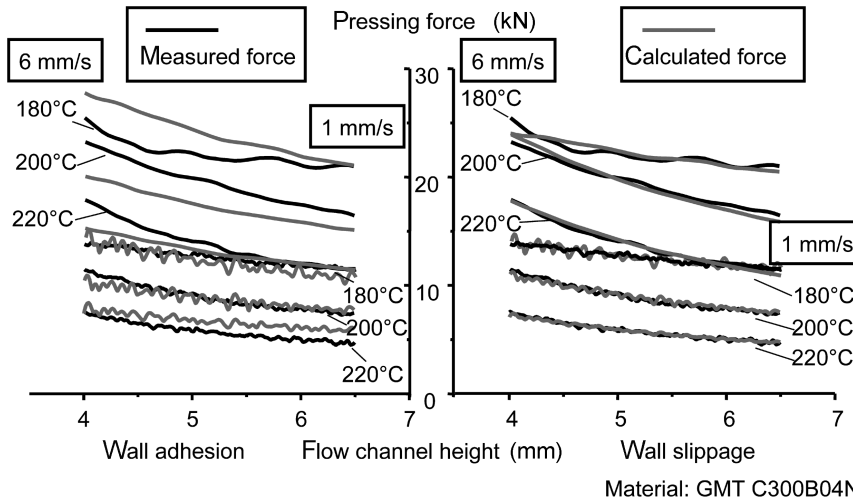

6.28 Press rheometer analysis: comparison of the analysis with wall adhesion and wall slippage effects (GMT).

6.5 References

Advani S G (1987), *Prediction of fibre orientation during processing of short fiber composites*, PhD Thesis at the University of Illinois at Urbana-Champaign.

Bush S F, Torres F G, Methven J M (2000) Rheological characterisation of discrete long glass fibre (LGF) reinforced thermoplastics, *Composites: Part A*, 31, 1421–1431.

Carreau P J (1968), *Rheological Equations from Molecular Network Theories*, PhD Thesis at the University of Wisconsin, Madison.

Diest K V (1996), *Prozeßsimulation und Faserorientierungserkennung von GMT-Bauteilen*, Aachen, Shaker Verlag.

Echaabi J, Trochu F, Gauvin R (1996), Review of failure criteria of fibrous composite materials, *Polymer Composites* 17, 786–798.

Ehrenstein G (1992), *Faserverbund-Kunststoffe, Werkstoffe-Verarbeitung-Eigenschaften*, München, Wien, Carl Hanser Verlag.

Folgar F (1983), *Fiber orientation distribution in concentrated suspensions: a predictive model*, PhD Thesis at the University of Illinois at Urbana-Champaign.

Folgar F, Tucker C L (1984), Orientation behavior of fibers in concentrated suspensions, *Journal of Reinforced Plastics and Composites*, 3, 98–119.

Heber M (1995), *Modell zur rheologischen Auslegung faserverstärkter, thermoplastischer Preßbauteile*, Aachen, Verlag Mainz.

Hele-Shaw H S, Stirling J (1899), The motion of a perfect liquid, *Nature*, 7 Sept. 1899, 107.

Jeffery G B (1922), The motion of ellipsoidal particles immersed in a viscous fluid *Proceedings of the Royal Society of London*, Series A, 102, 161–179.

Kamal M R, Sourour S (1973), Kinetics and thermal characterisation of thermoset cure, *Polymer Engineering and Science*, 13 (1), 59–64.

Michaeli W (1990), *Extrusionswerkzeuge für Kunststoffe*, München, Hanser Verlag.

Neitzel M, Breuer U (1996), *Die Verarbeitungstechnik der Faser-Kunststoff-Verbunde,* München, Wien, Carl Hanser Verlag.

Oelgarth A (1997), *Analyse und Charakterisierung des Fließverhaltens langfaser-verstärkter Preßmassen*, Aachen, Verlag Mainz.

Orgéas L, Le Corre S, Dumont P, Favier D, Tourabi A (2001), Influence of the fibre volume fraction and mechanical loading on the flow behaviour of sheet moulding compounds (SMC), *4th ESAFORM conference on material forming*, Liège, Belgium.

Osswald T (1987), *Numerical methods for compression mold filling simulation*, PhD Thesis at the University of Illinios at Urbana-Champaign.

Piry M (2004), *Mechanische Auslegung von SMC-Bauteilen und Charakterisierung der relevanten Werkstoffeigenschaften*, Aachen, Verlag Mainz.

Puck A (1967), Zur Beanspruchung und Verformung von GFK-Mehrschichtenverbund-Bauelementen Teil 1. Grundlagen der Spannungs- und Verformungsanalyse, *Kunststoffe*, 57, 4, 284–290.

Renz U (1989), *Grundlagen der Wärmeübertragung*, RWTH Aachen.

Ritter M (2003), *Materialcharakterisierung von Langfaserverstärkten Pressmassen und Beschreibung des Pressprozesses durch Simulation und Messung des Kraftschwer-punktverlaufs,* Aachen, Verlag Mainz.

Schmachtenberg E, Ritter M (2002), Quality assurance system based on the process simulation for the compression molding process, *SAMPE Conference, Long Beach California (USA)*.

Schmachtenberg E, Skrodolies K (2005), Process-simulation of compression moulding compounds, *Annual Technical Conference of the Society of Plastic Engineers (Antec),* Boston, MA, USA.

Schwarz H R (1986), *Numerische Mathematik*, Stuttgart, Teubner Verlag.

Semmler E (1998), *Simulation des mechanischen und thermomechanischen Verhaltens faserverstärkter thermoplastischer Pressmassen*, Aachen, Verlag Mainz.

Specker O (1990), *Pressen von SMC: Computersimulation zur rechnerunterstützten Auslegung des Prozesses und zur Ermittlung der Bauteileigenschaften*, Aachen, Fotodruck Mainz.

Williams M L, Landel R F, Fery J D (1955), The temperature dependence of relaxation mechanisms in amorphous liquids, *Journal of the American Chemical Society*, 77 (7), 3701–3706.

6.6 Symbols

a	[m/s]	Thermal diffusivity
a_T	[–]	Temperature shift factor
$c_{s,k}$	[–]	Degree of cure
d_F	[m]	Fibre (or fibre bundle) diameter
f_E	[m]	Failure factor
g	[m/s]	Gravitation
$\dot{h}$	[m/s]	Closing velocity
l_F	[m]	Fibre length
p	[Pa]	Pressure
r_E	[–]	Axis length ratio

t	[s]	Time
v	[m/s]	Velocity
x	[m]	Coordinate direction
y	[m]	Coordinate direction
z	[m]	Coordinate direction
C_l	[–]	Fibre interaction coefficient
E	[N/m^2]	Youngs modulus
G	[N/m^2]	Shear modulus
H	[m]	Flow channel height
P_1	[Pas]	Carreau parameter 1
P_2	[s^{-1}]	Carreau parameter 2
P_3	[–]	Carreau parameter 3
Q	[J/m^3]	Heat
$\dot{Q}$	[J/(m^{3}s)]	Rate of heat generation
R	[N/m^2]	Strength
S	[s/m^2]	Flow conductivity
T	[ºC]	Temperature
T_B	[ºC]	Reference temperature (WLF equation)
T_S	[ºC]	Standard temperature (WLF equation)
α	[W/(m^{2}K)]	Heat-transfer coefficient
λ	[W/(mK)]	Thermal conductivity
ρ	[kg/m^3]	Density
η	[Pas]	Viscosity
ν	[–]	Poissons ratio
ξ	[–]	Material and geometry parameter in the Halpin-Tsai Model
σ	[N/m^2]	Stress
τ	[Nm^2]	Shearing stress
ϕ	[º]	Angle
ψ	[–]	Fibre frequency
Φ	[–]	Fibre volume content
Ω	[–]	Grouping parameter
∇	[–]	Nabla operator